All-optical measurement of the hot electron sheath driving laser ion acceleration from thin foils

O Jäckel[1,2,6]**, J Polz**[1]**, S M Pfotenhauer**[1,3]**, H-P Schlenvoigt**[1,4]**, H Schwoerer**[1,5] **and M C Kaluza**[1,2]

[1] Institut für Optik und Quantenelektronik, Friedrich-Schiller-Universität, Max-Wien-Platz 1, 07743 Jena, Germany
[2] Helmholtz-Institut Jena, Helmholtzweg 4, 07743 Jena, Germany
E-mail: oliver.jaeckel2@uni-jena.de

Abstract. We present experimental results from an all-optical diagnostic method to directly measure the evolution of the hot-electron distribution driving the acceleration of ions from thin foils using high-intensity lasers. Central parameters of laser ion acceleration such as the hot-electron density, the temperature distribution and the conversion efficiency from laser pulse energy into hot electrons become comprehensively accessible with this technique.

[3] Current address: Massachusetts Institute of Technology, Cambridge, MA 02139-4307, USA.
[4] Current address: Laboratoire LULI, École Polytechnique, 91128 Palaiseau Cedex, France.
[5] Current address: Laser Research Institute, University of Stellenbosch, 7602 Matieland, South Africa.
[6] Author to whom any correspondence should be addressed.

IOP Institute of Physics   Φ DEUTSCHE PHYSIKALISCHE GESELLSCHAFT

Contents

1. Introduction

In recent years, high-intensity laser systems have proven to be promising candidates for next-generation particle accelerators [1, 2]. Laser-generated, relativistic plasmas can provide electric fields that are by several orders of magnitude stronger than the fields used in conventional accelerators and thus significantly reduce the particle acceleration length. In addition, it has been demonstrated that electron [3]–[7], proton [8, 9] and ion [10] pulses with monoenergetic features of a few per cent spectral bandwidth can be reliably generated, paving the way for possible applications (e.g. [11, 12]). Other unique properties of this source of energetic particles encompass ultrashort pulse duration [13]–[15] and excellent transverse and longitudinal emittances at the source [16] that allow for good focusability of the particle beams.

Until now, most improvements concerning particle properties have been achieved by improving the laser and target parameters. For example, enhancement of the maximum ion energy or spectral manipulation can be achieved by employing special target designs using microstructured [8, 9, 17] or nanolayered thin foils [10, 18], ultrathin foils [19]–[21] and droplet targets [22, 23] or by employing subsequent beam shaping devices such as fs-gated, electrostatic focusing optics as a so-called laser-driven microlens [24] or cascaded acceleration setups [25]. All these approaches follow theoretical models about the nature of the underlying physical processes. Although these models were continuously refined in accordance with novel experimental findings, no adequate real-time observation tool has been available for studying the interaction and thus the acceleration itself. So far, proton deflectometry is the only diagnostic capable of resolving the relevant physical processes leading to laser ion acceleration by measuring the electric fields within the electron sheath [26]–[30]. However, proton deflectometry is constrained by picosecond temporal resolution, insufficient for tracking the rapid, femtosecond-scale laser plasma dynamics responsible for particle acceleration, and requires a complicated setup of two correlated laser accelerators to probe the generation of one particle beam with the other. This mismatch has repeatedly led to calls for improvement of diagnostics to better understand the nature of laser particle acceleration.

Here we present an all-optical method for directly probing and reconstructing the electron distribution that drives laser ion acceleration from thin foils in real time. The use of an optical probe pulse of 100 fs pulse duration offers an unprecedented temporal resolution operating on

the theoretically predicted time scale of the acceleration process determined by the duration of the driving laser pulse [14, 29].

2. The TNSA process

The process responsible for efficient laser-ion acceleration from μm-thin foils is generally known as target normal sheath acceleration (TNSA) [31]. Different acceleration regimes become important when using ultrahigh-power lasers ($\geqslant 100$ TW) and ultrathin foils ($\leqslant 100$ nm) [19, 21], gas jets [32]–[34] or foam targets [35].

A laser pulse (with intensity I_L) impinges on the front surface of a thin foil of μm thickness and generates—mainly via ponderomotive acceleration—a hot-electron component that propagates through the target foil. The majority of these electrons are trapped in the electric potential ϕ arising from the charge separation. Thus, the hot electrons can be described by a Boltzmann distribution $n_e(z) = n_{e0} \exp\{e\phi(z)/k_B T_e\}$, where the hot-electron temperature $k_B T_e = \Phi_P$ is determined by using the ponderomotive potential $\Phi_P = m_e c^2 ((1 + I_L \lambda_L^2 / 1.37 \times 10^{18}\,\mathrm{W\,cm^{-2}\,\mu m^2})^{1/2} - 1)$ of the laser pulse, with I_L and λ_L being the laser intensity and wavelength, respectively. n_{e0} is the hot-electron density inside the target foil and e is the elementary charge.

Under these conditions, the electron density n_e follows an exponentially decaying density distribution in the longitudinal direction (normal to the target rear surface) behind the target foil related to the Debye length $\lambda_D = (\epsilon_0 k_B T_e / e^2 n_e)^{1/2}$. For $t = 0$, an analytical solution of the Poisson equation can be derived outside the target foil ($n_{i0}(z > 0) = 0$) for the one-dimensional (1D) case [36]:

$$n_e(z > 0) = n_{e0} \exp\left\{-2\ln\left(1 + z/\sqrt{2e_N}\lambda_D\right) - 1\right\}, \tag{1}$$

where e_N is Euler's number.

In simple estimations, the radial extent w_{n_e} (full-width at half-maximum (FWHM)) of this electron sheath has so far been calculated using the focal spot size on the target front surface, d_{foc} (FWHM), while assuming a ballistic propagation of the hot electrons through the target. For a target thickness of d_t and an electron half-opening angle of θ, this leads to $w_{n_e} = (d_{\mathrm{foc}} + 2d_t \tan\theta)$ [37]. The electron propagation through the target can be assumed to be symmetric around the target normal direction for a sufficiently short front-surface plasma scale length even for oblique incidence of the driving laser pulse on the target front surface [38, 39]. Previous measurements of the contrast ratio of the laser system allow us to conclude that the front-surface scale length is shorter than λ_L.

In contrast to the transverse diameter of the rear-surface electron sheath estimated from the laser focal spot size, a significantly larger diameter can be expected because of effects such as electron recirculation [40] or the fountain effect [41]–[44] that are not included in the above-mentioned simple estimations, leading to a larger source size of the accelerated ions [45]. However, in the case of normal electron propagation through the target, it can be expected that the rear-surface electron sheath still preserves its cylindrical symmetry with respect to the target normal. For sufficiently large aspect ratios (i.e. the ratio of the extent of the electron sheath in the target normal direction and the lateral diameter of the sheath), the generated electric fields can still be approximated using the above-mentioned 1D model.

Within the cloud of hot electrons at the rear surface a strong electric field $E_{\mathrm{TNSA}} = -\partial\phi(z)/\partial z|_{z=0} = \sqrt{2/e_N}\sqrt{k_B T_e n_e/\epsilon_0}$ is generated, which ionizes atoms at the target rear

surface immediately [46]. Once these ions have been generated they are accelerated normally to the target surface up to MeV energies. As the acceleration is sensitive to the charge to mass ratio q/m, protons are accelerated most effectively.

The electric field in the sheath is mainly determined by the distributions of number density and temperature of the electrons. Although it is likely that the total electron distribution is a combination of more than one temperature component, only the hottest-electron component can leak out of the target rear surface over distances of $1\,\mu$m or higher [41, 47] at the beginning of the ion acceleration process. While at later times the less energetic electrons can also leave the target, the density distribution of the ions still exhibits a very steep, almost step-like density distribution at these early times. Due to their Debye length in the nm range, the extent of the low-temperature electron component at the target rear surface is only tens of nanometers and this is not resolvable with the present setup. Although the low-temperature component may increase the electric field strength close to the target rear surface, the electric field in the electron cloud is determined only by the hot-electron component.

Typical estimations following the geometrical assumptions concerning the electron sheath extent with an electron beam divergence half-angle of $\theta \approx 8°$ [48] as well as an energy conversion of laser light into hot electrons of 10% lead to $n_{e0} = 9.4 \times 10^{19}\,\text{cm}^{-3}$ [14, 37]. Together with $I_L = 0.94 \times 10^{19}\,\text{W cm}^{-2}$, one expects that $k_B T_e = 0.7\,\text{MeV}$, $\lambda_D = 0.6\,\mu$m and $w_{n_e} = 8.6\,\mu$m for the conditions of our experiment. Consequently, the ionizing and accelerating electric field strength is $1.1\,\text{TV m}^{-1}$. To test the validity of these estimations experimentally, a diagnostic sensitive to the electron distribution with high spatial (of the order of microns) and temporal resolution (of the order of the laser pulse duration) is necessary.

3. Experimental setup

The experiments have been carried out at the Jena 10 TW titanium:sapphire laser system JETI, which delivered pulses of $E_L = 500\,\text{mJ}$ within $\tau_L = 80\,\text{fs}$ (FWHM) at a central wavelength of $\lambda_L = 800\,\text{nm}$. An $f/2$ off-axis parabolic gold mirror focused the laser pulses into a focal spot of $A_L = 11.5\,\mu\text{m}^2$ (FWHM), which contained 30% of the energy, leading to intensities of $I_L = 1.1 \times 10^{19}\,\text{W cm}^{-2}$ on the target taking into account the incidence angle of 45°. The probe beam was separated from the compressed main pulse, telescoped down to a diameter of 1 mm and frequency-doubled using a BBO crystal. Due to the additionally accumulated optical path length, the final pulse duration of the probe pulse on the target was $\tau_{2\omega} \approx 100\,\text{fs}$ owing to group velocity dispersion. A variable delay line with a minimum step size of 66 fs allowed us to choose different probing times within a time window of 4 ns around the arrival of the peak of the main pulse on the target front surface. Figure 1 shows a schematic overview of the setup. Titanium foils of $d_t = 6\,\mu$m thickness were mounted on specially bent target frames (radius of curvature 5 cm). The 2ω probe pulse passed the curved rear surface of the target tangentially and collected a phase shift $\Delta\Phi \approx \omega_L/(2cn_c) \int n_e \, ds$ ($n_e \ll n_c$) during its propagation through the electron sheath. Here ω_L and c are the laser frequency and the speed of light, respectively; $n_c = \epsilon_0 m_e \omega_L^2/e^2$ is the critical density.

A Nomarski interferometer comprising a Wollaston prism (separation angle 1°) and a polarizer imaged the region of interest onto a 12 -bit CCD camera using a high-quality $f/2$ lens. The $1.1\,\mu$m spatial resolution of this setup was found to be close to the diffraction limit using a standard resolution test pattern. The evaluation of the interferograms was performed using IDEA software [49]. Assuming cylindrical symmetry of the rear-surface plasma with respect to
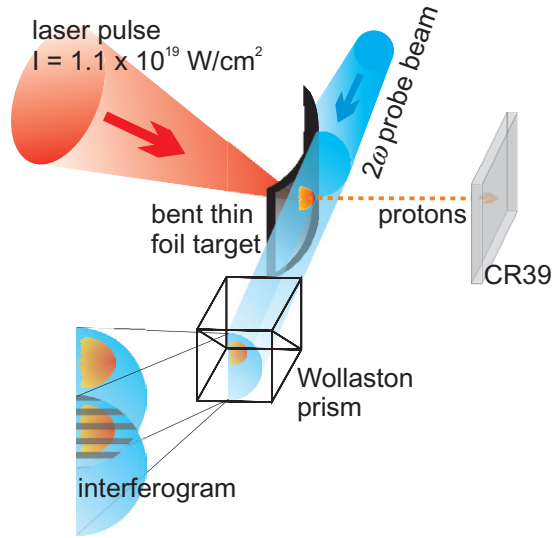
Figure 1. Schematic overview of the experimental setup.

the target normal direction, the absolute electron density distribution could be obtained from the phase shift plots via an Abel inversion. The ellipticity of the rear-surface sheath was confirmed to be smaller than 1:1.3 by a different setup using reflectivity probing of the rear surface.

The target foils were $25 \times 25 \, \text{mm}^2$ in size. A custom-designed translation and rotation stage arrangement allowed us to take up to 40 shots onto each foil without breaking the vacuum. A robust alignment procedure guaranteed that the main laser pulse hit the foil exactly at the osculation point of the tangential probe beam. The accuracy of the alignment corresponds to a maximum shaded region of $0.1 \, \mu\text{m}$ thickness in the target normal direction, which might not have been accessible by our imaging system.

In order to determine the proton energy, a CR39 nuclear track detection plastic positioned 15 cm behind the target foil on the target normal axis was covered with aluminum filter strips of increasing thickness towards the beam center.

4. Results of the optical probing of laser ion acceleration from thin foils

4.1. Properties of the initial electron density distribution

Figure 2 shows the density distribution of the rear-surface electron sheath recorded at $t = 0$. The time $t = 0$ refers to the *first* moment when a signal can be detected on the target rear surface after successively moving the delay stage towards earlier times in steps of 66 fs. The electron distribution shows an exponential decay with a half-value length of $1.5 \, \mu\text{m}$ from $n_\text{e} = 3 \times 10^{19}$ to $0.5 \times 10^{19} \, \text{cm}^{-3}$ over a distance of $7.5 \, \mu\text{m}$ in the target normal direction as well as a Gaussian shape in the radial direction with $21 \, \mu\text{m}$ FWHM.

Applying equation (1), the density distribution was approximated by an exponential drop in the longitudinal direction described by a Debye length of $\lambda_\text{D} = (1.0 \pm 0.2) \, \mu\text{m}$ and a hot-electron density inside the target of $n_\text{e0} = (8.4 \pm 0.4) \times 10^{19} \, \text{cm}^{-3}$ directly from the measured data. The errors have been determined by analyzing different shots taken under the same
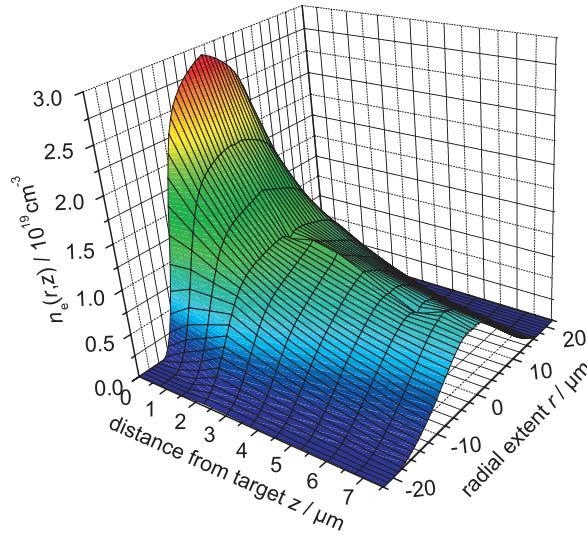
Figure 2. Electron density distribution of the electron sheath at the rear surface of the target foil recorded at a time step t_0.

experimental conditions, by determining the influence of parameters that are necessary to initialize the Abel inversion and, finally, by the deviation of the deduced values from the theoretical fit curve that is given by equation (1).

The density profile is in good agreement with the predictions of the theoretical model. The experimentally determined electron density and scale length differ slightly from the theoretical values in terms of absolute numbers: n_{e0} is overestimated by 12%, leading to a 40% smaller predicted value of λ_D. The same is true for the electron temperature, which was deduced to be $k_B T_e = (1.5 \pm 0.4)\,\text{MeV}$, in contrast to the value given by the ponderomotive potential of the laser which is smaller by a factor of 2. The initial electric field strength derived from our measurements of $E_{TNSA} = (1.1 \pm 0.4)\,\text{TV m}^{-1}$ is found to be in good agreement with the theoretical model as the effects from the higher temperature and the smaller Debye length tend to compensate each other.

Note that the experimentally measured initial distribution of n_e can, to first order, be approximated to be 1D, i.e. its decay in the z direction is much faster than that in the radial direction with an aspect ratio of 1:14 given by the half-values, which justifies the application of the analytical solutions of the 1D model [36, 50].

4.2. Efficiency of energy conversion

A parameter of central interest for understanding the interaction process is the energy conversion efficiency η of laser light into hot electrons: $\eta = N_e k_B T_e / E_L$. The values from the literature vary between a few per cent and several ten per cent, and were also predicted to follow an intensity scaling $\eta = 1.2 \times 10^{-15} I_L^{0.75}$ [14, 51, 52]. From our measurements, we can deduce the energy of the electrons in the rear-surface sheath E_{Sheath} directly by integrating the number density over space to obtain the total number of sheath electrons $N_{Sheath} = (5.1 \pm 0.1) \times 10^{10}$ and multiplying it by their deduced average temperature $k_B T_e = (1.5 \pm 0.4)\,\text{MeV}$.

This leads to $E_{\text{Sheath}} = (12 \pm 4)$ mJ, which would correspond to a conversion efficiency of $\eta_{\text{Sheath}} = (2.6 \pm 0.8)\%$. The total conversion efficiency of laser light into hot electrons can be deduced by the following estimation. We assume that, after being accelerated by the laser, the hot electrons occupy a cylindrical volume V inside the target of $V = d_{\text{t}} \pi (w_{n_{\text{e}}}/2)^2$, where d_{t} and $w_{n_{\text{e}}}$ are the target thickness and the radial extent of the rear surface sheath, respectively. Multiplying this volume by the hot electron density inside the target n_{e0} and their temperature $k_{\text{B}}T_{\text{e}}$ that we deduced from our measurements yields a total energy of the hot electrons of $E_{\text{hot}} = (42 \pm 13)$ mJ. Using this estimated number, the conversion efficiency of laser energy into hot electrons is $\eta = (9.1 \pm 2.8)\%$. This value is in good agreement with the literature; however, it does not support the intensity scaling $\eta(I_{\text{L}} = 1.1 \times 10^{19} \, \text{W} \, \text{cm}^{-2}) = 23\%$ as mentioned in [14, 51, 52]. Note that for the determination of this value we took into account only that part of the electron population exhibiting the highest quasi-temperature.

A comparison with 3D-PIC (particle-in-cell) simulations by Pukhov [41] supports our experimental results strongly. For comparable laser and target conditions ($I_{\text{L,sim}} = 10^{19} \, \text{W} \, \text{cm}^{-2}$, $d_{\text{t,sim}} = 12 \, \mu\text{m}$), an electron sheath of $20 \, \mu\text{m} \times 6 \, \mu\text{m}$ radial to longitudinal extent is found, strikingly similar to our experimental results. The simulation yields a slightly higher initial electron density of a few $10^{20} \, \text{cm}^{-3}$, which might be ascribed to differences in the electron transport or the conversion efficiency of laser light into hot electrons assumed for the numerical modelling.

Since the numerical simulation results also support the result of our measurement of the radial extent of the electron density distribution $w_{n_{\text{e}}} = 21 \, \mu\text{m}$ in contrast to the simple estimation for $w_{n_{\text{e}}} = 8.6 \, \mu\text{m}$ due to electrons propagating ballistically through the target, this might point to an experimental observation of the so-called fountain effect [41]–[44]. A magnetically collimated electron beam leaving the back of the target spreads and is drawn back towards the surface and this causes a rapid broadening of the electron density distribution.

4.3. Duration of ion acceleration

Differently filtered CR39 plates show proton energies larger than 2.9 MeV, which is also supported by previous measurements with an ion spectrometer [8, 9] in a similar setup, where proton cutoff energies of 4 MeV were measured. This observed maximum energy can be used to estimate the effective acceleration time of the protons in the TNSA sheath field—a parameter of central importance to many theoretical models.

Figure 3 shows a plot of the maximum proton energy acquired by a proton propagating through the sheath field caused by the electron distribution of figure 2 as a black line, which was obtained by solving the 1D equation of motion numerically. This plot is contrasted with the plasma expansion model displayed as a gray line [50], again using the experimental results of electron temperature and density. For early acceleration times we find very good agreement between the two models. However, after approximately 300 fs, a discrepancy occurs due to negligence of the ion front expansion in the simple quasi-static 1D approach.

The measured maximum proton energy of $E_{\text{max}} \geqslant 2.9$ MeV corresponds to an acceleration time of $\tau_{\text{acc,meas}} \geqslant 280$ fs, which is in excellent accord with estimates by Fuchs *et al* $\tau_{\text{acc}} \leqslant 2.5 \, (\tau_{\text{L}} + 60 \, \text{fs}) \approx 350$ fs based on a refined theoretical model and a proton energy scan for different laser parameters [29]. Our findings confirm this long-standing model by using a direct experimental probing technique.
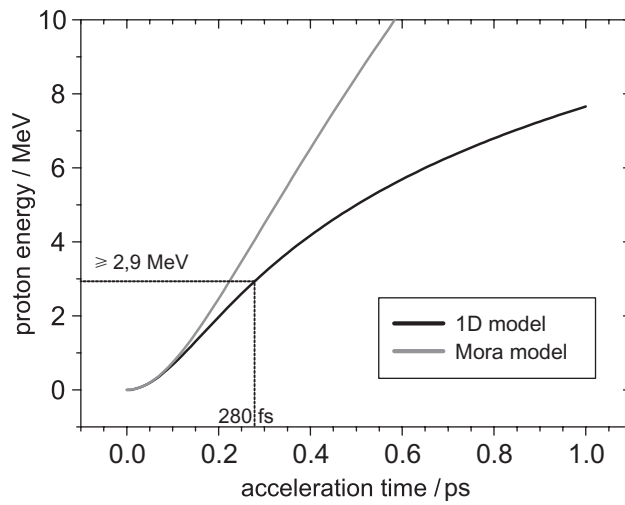
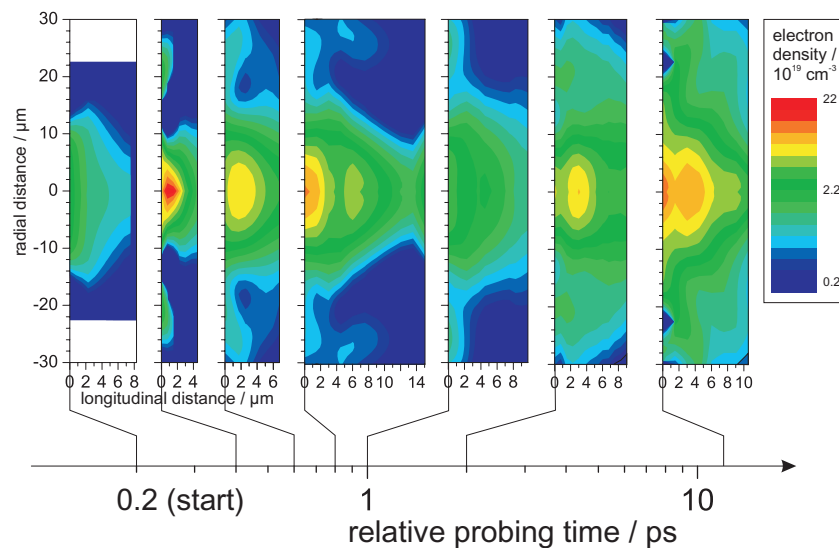**Figure 3.** Maximum proton energy versus acceleration time.

Figure 4. Temporal evolution of the electron density at the rear surface of the target. All pictures are shifted +200 fs due to the logarithmic time scale.

4.4. Temporal evolution of the electron sheath

Varying the delay of the probe pulse with respect to the main pulse, the temporal evolution of the electron sheath has been studied as shown in figure 4 on a logarithmic time scale. Note the offset of 0.2 ps due to the logarithmic scale. For early times up to 0.8 ps, the electron sheath expands almost only in the target normal direction. The expansion in the transverse direction becomes more significant for later probing times starting from about 1 ps. The maximum number density rapidly increases with the second time step and remains at comparable high values with a dip at 1.0 ps for the whole range of observation until 10 ps.
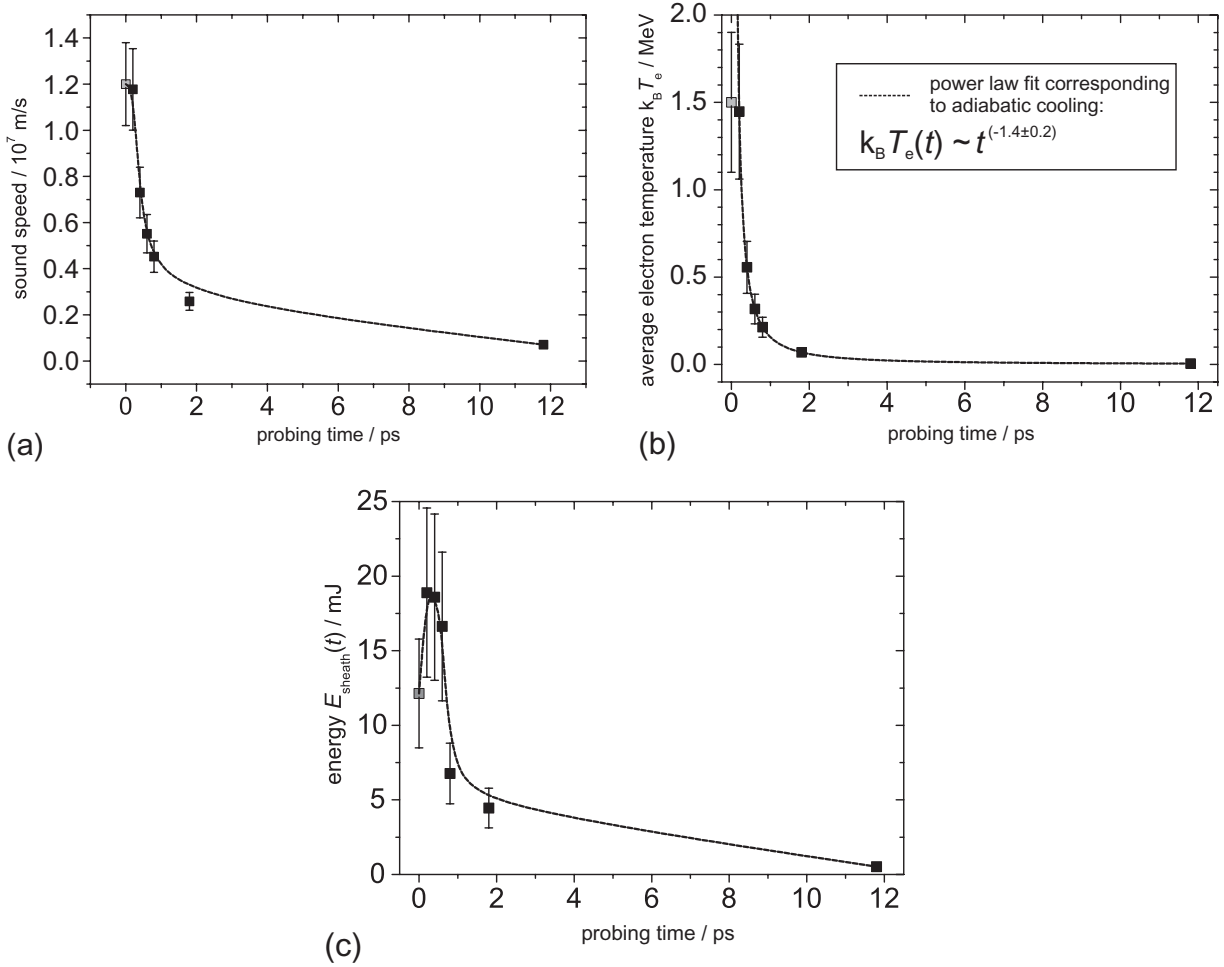
Figure 5. Properties of the electron sheath as a function of time. (a) Sound speed $c_s(t)$. (b) Electron temperature $k_B T_e(t)$. (c) Energy content $E_{sheath}(t)$. The gray squares refer to the results evaluated via the analytical model at $t = 0$ and the black squares are deduced from the sheath expansion evaluation. The dashed lines in (a) and (c) are a guide to the eye.

Since the analytical description of the longitudinal decay of $n_e(z)$ is valid only for $t = 0$, we assume the self-similar expansion of a hydrogen plasma into vacuum in order to model our observations. We further assume that the electron density profile expands with the ion sound speed $\dot{z}(t, n_e = \text{const}) = c_s(t) = (Z k_B T_e(t)/m_i)^{1/2}$ and, hence, contains information on the momentary hot-electron temperature. The results of this approach are shown in figure 5. Its relative uncertainty was determined to be less than 30%.

The expansion velocity is found to decrease with time, indicating a deceleration of the plasma expansion. This behavior is expected owing to cooling of the hot-electron population driving the expansion. In particular, the rapid decrease of the electron temperature in figure 5(b) indicates the adiabatic cooling behavior expected from an expanding plasma [53]. For later times, we find that $k_B T_e \sim t^{-(1.4\pm0.2)}$ as shown by the gray line. This exponential fit is in accord with numerical simulations by Mora [53] and falls into the transition between the limits of ultra-relativistic ($k_B T_e \sim t^{-1}$) and nonrelativistic ($k_B T_e \sim t^{-2}$) electron description. Thus, it strongly

supports the description of the TNSA process as an adiabatic expansion of a plasma at the rear surface of a thin foil at later times.

For the hot-electron temperature, relativistic values were found for the first three time steps up to 400 fs only. From this upper limit for the duration of a relativistic interaction, one can make further predictions about the acceleration time period that can be narrowed down further to 280 fs $\leqslant \tau_{acc} \leqslant$ 400 fs in accord with the predictions in [29].

In figure 5(c), the energy content of each electron density plot is evaluated over time assuming the above-calculated hot-electron temperature. We find that the energy contained by the sheath peaks at 200 fs, corresponding to a slightly higher energy portion of $\eta_{Sheath} = (4.1 \pm 1.2)\%$ at that time than reported above. This value marks an upper boundary for the energy transfer into the ions, which is in good agreement with table 1 of [54].

5. Conclusion

We have presented the experimental results from an all-optical scheme for the direct measurement of the electron distribution driving the laser ion acceleration from thin foils. The use of a synchronized probe beam and a special target geometry enabled temporal and spatial resolution a factor of 10 better than previous measurements made with proton deflectometry or ps laser pulses. This setup allows direct deduction of the Debye length $\lambda_D = (1.0 \pm 0.2)\,\mu m$ and the undisturbed electron density inside the target $n_{e0} = (8.4 \pm 0.4) \times 10^{19}\,cm^{-3}$, as well as calculation of the hot-electron temperature $k_B T_e = (1.5 \pm 0.4)\,MeV$ at the point in time when the acceleration process starts. The results are strongly supported by 3D-PIC simulations [41] and confirm the acceleration time prediction of Fuchs *et al* [29] regarding the maximum proton energy. Finally, a time-resolved measurement of the electron sheath highlighted the adiabatic nature of the cooling of the electron population and allowed determination of the energy conversion of laser light into hot electrons of the sheath to be $\eta_{Sheath} = (4.1 \pm 1.2)\%$. The total conversion efficiency into hot electrons has been estimated as $\eta = (9.1 \pm 2.8)\%$. The proposed setup is, in principle, transferable to any other laser ion acceleration experiment under the stipulation that the targets can be bent or the rear surface can be made accessible in any other way, which is the case for most of the proposed target improvements.

Making direct, quantitative measurements of the electron sheath that drives ion acceleration from thin foils adds significantly to the understanding of laser ion acceleration and the underlying physics. In the future, it might help in improving the parameters of the generated particle pulses, which is a prerequisite for a large number of envisaged applications.

Acknowledgments

References

[1] Umstadter D 2001 Review of physics and applications of relativistic plasmas driven by ultra-intense lasers *Phys. Plasmas* **8** 1774–85
[2] Mourou G A, Tajima T and Bulanov S V 2006 Optics in the relativistic regime *Rev. Mod. Phys.* **78** 309–71

[3] Faure J, Glinec Y, Pukhov A, Kiselev S, Gordienko S, Lefebvre E, Rousseau J P, Burgy F and Malka V 2004 A laser–plasma accelerator producing monoenergetic electron beams *Nature* **431** 541–4

[4] Geddes C G R, Toth C, van Tilborg J, Esarey E, Schroeder C B, Bruhwiler D, Nieter C, Cary J and Leemans W P 2004 High-quality electron beams from a laser wakefield accelerator using plasma-channel guiding *Nature* **431** 538–41

[5] Mangles S P D *et al* 2004 Monoenergetic beams of relativistic electrons from intense laser–plasma interactions *Nature* **431** 535–8

[6] Hidding B *et al* 2006 Generation of quasimonoenergetic electron bunches with 80-fs laser pulses *Phys. Rev. Lett.* **96** 105004

[7] Leemans W P, Nagler B, Gonsalves A J, Toth C, Nakamura K, Geddes C G R, Esarey E, Schroeder C B and Hooker S M 2006 GeV electron beams from a centimetre-scale accelerator *Nature Phys.* **2** 696–9

[8] Schwoerer H, Pfotenhauer S, Jäckel O, Amthor K U, Liesfeld B, Ziegler W, Sauerbrey R, Ledingham K W D and Esirkepov T 2006 Laser–plasma acceleration of quasi-monoenergetic protons from microstructured targets *Nature* **439** 445–8

[9] Pfotenhauer S M *et al* 2008 Spectral shaping of laser generated proton beams *New J. Phys.* **10** 33034

[10] Hegelich B M, Albright B J, Cobble J, Flippo K, Letzring S, Paffett M, Ruhl H, Schreiber J, Schulze R K and Fernandez J C 2006 Laser acceleration of quasi-monoenergetic MeV ion beams *Nature* **439** 441–4

[11] Schlenvoigt H P *et al* 2008 A compact synchrotron radiation source driven by a laser–plasma wakefield accelerator *Nature Phys.* **4** 130–3

[12] Fuchs M *et al* 2009 Laser-driven soft-x-ray undulator source *Nature Phys.* **5** 826–9

[13] van Tilborg J, Schroeder C B, Filip C V, Toth C, Geddes C G R, Fubiani G, Huber R, Kaindl R A, Esarey E and Leemans W P 2006 Temporal characterization of femtosecond laser–plasma-accelerated electron bunches using terahertz radiation *Phys. Rev. Lett.* **96** 014801

[14] Fuchs J *et al* 2006 Laser-driven proton scaling laws and new paths towards energy increase *Nature Phys.* **2** 48–54

[15] Debus A D *et al* 2010 Electron bunch length measurements from laser-accelerated electrons using single-shot THz time-domain interferometry *Phys. Rev. Lett.* **104** 084802

[16] Cowan T E *et al* 2004 Ultralow emittance, multi-MeV proton beams from a laser virtual-cathode plasma accelerator *Phys. Rev. Lett.* **92** 204801

[17] Esirkepov T Zh *et al* 2002 Proposed double-layer target for the generation of high-quality laser-accelerated ion beams *Phys. Rev. Lett.* **89** 175003

[18] Albright B J, Yin L, Hegelich B M, Bowers K J, Kwan T J T and Fernández J C 2006 Theory of laser acceleration of light-ion beams from interaction of ultrahigh-intensity lasers with layered targets *Phys. Rev. Lett.* **97** 115002

[19] Henig A *et al* 2009 Radiation-pressure acceleration of ion beams driven by circularly polarized laser pulses *Phys. Rev. Lett.* **103** 245003

[20] Esirkepov T, Borghesi M, Bulanov S V, Mourou G and Tajima T 2004 Highly efficient relativistic-ion generation in the laser-piston regime *Phys. Rev. Lett.* **92** 175003

[21] Robinson A P L, Zepf M, Kar S, Evans R G and Bellei C 2008 Radiation pressure acceleration of thin foils with circularly polarized laser pulses *New J. Phys.* **10** 013021

[22] Ter-Avetisyan S, Schnürer M, Nickles P V, Kalashnikov M, Risse E, Sokollik T, Sandner W, Andreev A and Tikhonchuk T 2006 Quasimonoenergetic deuteron bursts produced by ultraintense laser pulses *Phys. Rev. Lett.* **96** 145006

[23] Brantov A V, Tikhonchuk V T, Klimo O, Romanov D V, Ter-Avetisyan S, Schnürer M, Sokollik T and Nickles P V 2006 Quasi-mono-energetic ion acceleration from a homogeneous composite target by an intense laser pulse *Phys. Plasmas* **13** 122705

[24] Toncian T *et al* 2006 Ultrafast laser-driven microlens to focus and energy-select mega-electron volt protons *Science* **312** 410–3

[25] Pfotenhauer S M, Jäckel O, Polz J, Steinke S, Schlenvoigt H P, Heymann J, Robinson A P and Kaluza M C 2010 A cascaded laser acceleration scheme for the generation of spectrally controlled proton beams *New J. Phys.* **12** 103009

[26] Borghesi M, Campbell D H, Schiavi A, Willi O, Mackinnon A J, Hicks D, Patel P, Gizzi L A, Galimberti M and Clarke R J 2002 Laser-produced protons and their application as a particle probe *Laser Part. Beams* **20** 269–75

[27] Borghesi M *et al* 2005 High-intensity laser–plasma interaction studies employing laser-driven proton probes *Laser Part. Beams* **23** 291–5

[28] Romagnani L *et al* 2005 Dynamics of electric fields driving the laser acceleration of multi-MeV protons *Phys. Rev. Lett.* **95** 195001

[29] Fuchs J *et al* 2007 Comparative spectra and efficiencies of ions laser-accelerated forward from the front and rear surfaces of thin solid foils *Phys. Plasmas* **14** 053105

[30] Sokollik T *et al* 2008 Transient electric fields in laser plasmas observed by proton streak deflectometry *Appl. Phys. Let.* **92** 091503

[31] Wilks S C, Langdon A B, Cowan T E, Roth M, Singh M, Hatchett S, Key M H, Pennington D, MacKinnon A and Snavely R A 2001 Energetic proton generation in ultra-intense laser–solid interactions *Phys. Plasmas* **8** 542–9

[32] Krushelnick K *et al* 1999 Multi-MeV ion production from high-intensity laser interactions with underdense plasmas *Phys. Rev. Lett.* **82** 737

[33] Wei M S *et al* 2004 Ion acceleration by collisionless shocks in high-intensity-laser–underdense-plasma interaction *Phys. Rev. Lett.* **93** 155003

[34] Willingale L *et al* 2006 Collimated multi-MeV ion beams from high-intensity laser interactions with underdense plasma *Phys. Rev. Lett.* **96** 245002
Willingale L *et al* 2007 Reply *Phys. Rev. Lett.* **98** 049504

[35] Willingale L *et al* 2009 Characterization of high-intensity laser propagation in the relativistic transparent regime through measurements of energetic proton beams *Phys. Rev. Lett.* **102** 125002

[36] Crow J E, Auer P L and Allen J E 1975 Expansion of a plasma into a vacuum *J. Plasma Phys.* **14** 65–76

[37] Kaluza M, Schreiber J, Santala M I K, Tsakiris G D, Eidmann K, Meyer-ter Vehn J and Witte K J 2004 Influence of the laser prepulse on proton acceleration in thin-foil experiments *Phys. Rev. Lett.* **93** 045003

[38] Ruhl H, Sentoku Y, Mima K, Tanaka K A and Kodama R 1999 Collimated electron jets by intense laser-beam plasma surface interaction under oblique incidence *Phys. Rev. Lett.* **82** 743

[39] Santala M I K *et al* 2000 Effect of the plasma density scale length on the direction of fast electrons in relativistic laser–solid interactions *Phys. Rev. Lett.* **84** 1459

[40] Mackinnon A J, Sentoku Y, Patel P K, Price D W, Hatchett S, Key M H, Andersen C, Snavely R and Freeman R R 2002 Enhancement of proton acceleration by hot-electron recirculation in thin foils irradiated by ultraintense laser pulses *Phys. Rev. Lett.* **88** 215006

[41] Pukhov A 2001 Three-dimensional simulations of ion acceleration from a foil irradiated by a short-pulse laser *Phys. Rev. Lett.* **86** 3562–5

[42] Tikhonchuk V T 2002 Interaction of a beam of fast electrons with solids *Phys. Plasmas* **9** 1416–21

[43] Robinson A P L and Sherlock M 2007 Magnetic collimation of fast electrons produced by ultraintense laser irradiation by structuring the target composition *Phys. Plasmas* **14** 083105

[44] Yogo A *et al* 2008 Laser ion acceleration via control of the near-critical density target *Phys. Rev.* E **77** 016401

[45] Schreiber J *et al* 2004 Source-size measurements and charge distributions of ions accelerated from thin foils irradiated by high-intensity laser pulses *Appl. Phys.* B **79** 1041–5

[46] Hegelich M *et al* 2002 MeV ion jets from short-pulse-laser interaction with thin foils *Phys. Rev. Lett.* **89** 085002

[47] Passoni M, Tikhonchuk V T, Lontano M and Yu B V 2004 Charge separation effects in solid targets and ion acceleration with a two-temperature electron distribution *Phys. Rev.* E **69** 026411

[48] Honrubia J J, Kaluza M, Schreiber J, Tsakiris G D and Meyer-ter Vehn J 2005 Laser-driven fast-electron transport in preheated foil targets *Phys. Plasmas* **12** 052708

IOP Institute of Physics ⦿ DEUTSCHE PHYSIKALISCHE GESELLSCHAFT

[49] Hipp M, Woisetschläger J, Reiterer P and Neger T 2004 Digital evaluation of interferograms *Measurement* **36** 53–66
   IDEA—interferometric data evaluation algorithms http://optics.tu-graz.ac.at/idea/idea.html

[50] Mora P 2003 Plasma expansion into a vacuum *Phys. Rev. Lett.* **90** 185002

[51] Key M H *et al* 1998 Hot electron production and heating by hot electrons in fast ignitor research *Phys. Plasmas* **5** 1966–72

[52] Yu J, Jiang Z, Kieffer J and Krol A 1999 Hard x-ray emission in high intensity femtosecond laser–target interaction *Phys. Plasmas* **6** 1318–22

[53] Mora P 2005 Thin-foil expansion into a vacuum *Phys. Rev.* E **72** 056401

[54] Borghesi M, Fuchs J, Bulanov S V, Mackinnon A J, Patel P K and Roth M 2006 Fast ion generation by high-intensity laser irradiation of solid targets and applications *Fusion Sci. Technol.* **49** 412–39